Geochemical differences between alive, uncrusted and dead, crusted shells of Neogloboquadrina pachyderma: Implications for paleoreconstruction Brittany N. Hupp^{1,2,3} and Jennifer S. Fehrenbacher² ¹NOAA Climate and Global Change Postdoctoral Fellowship Program, CPAESS, UCAR, Boulder, CO, USA ²College of Earth, Ocean, and Atmospheric Sciences, Oregon State University, Corvallis, OR 97331 USA ³Department of Atmospheric, Oceanic and Earth Sciences, George Mason University, Fairfax, VA 22030 USA Corresponding Author: Brittany N. Hupp (bhupp@gmu.edu) Key Points: The gametogenic crust of planktic foraminifera have lower trace elements compared to uncrusted shells collected from the same surface tow. • Stable isotope comparisons indicate that foraminifera develop crusts deeper in the water column than their average living depth habitat. • Application of culture calibrations from TE-enriched uncrusted shells to crusted fossil records may produce inaccurate paleoreconstructions. Key words: planktic foraminifera, vital effects, trace element geochemistry, crust, gametogenesis, biomineralization

Abstract

31

32

33

34

35

36

37

38

39

40

41

42

43

44

45

46

47

48

Planktic foraminiferal-based trace element-calcium ratios (TE/Ca) are a cornerstone in paleoceanographic reconstructions. While TE-environment calibrations are often established through culturing experiments, shell growth in culture is not always consistent with growth in a natural setting. For example, many species of planktic foraminifera thicken their shell at the end of their life cycle, producing a distinct 'gametogenic' crust. Crust is common in fossil foraminifers, however, shells grown in culture do not often develop a thick crust. Here we investigate potential vital effects associated with the crusting process by comparing the trace element (Mg/Ca, Na/Ca, Ba/Ca, Sr/Ca, Mn/Ca, Zn/Ca) and stable isotope (δ¹³C, δ¹⁸O) composition of alive, fully mature, uncrusted shells to recently deceased, crusted shells of Neogloboquadrina pachyderma collected from the same plankton tows off the Oregon (USA) coast. We find that uncrusted (N = 55) shells yield significantly higher Ba/Ca, Na/Ca, Mn/Ca, and Sr/Ca than crusted (N = 66) shells, and crust calcite records significantly lower TE/Ca values for all elements examined. Isotopic mixing models suggest that the crust calcite accounts for ~40 to 70% of crusted shell volume. Comparison of foraminiferal and seawater isotopes indicate that N. pachyderma lives in the upper 90 m of the water column, and that crust formation occurs slightly deeper than their average living depth habitat. Results highlight the necessity to establish calibrations from crusted shells, as application of calibrations from TE-enriched uncrusted shells may yield attenuated or misleading paleoceanographic reconstructions.

4950

51

52

53

54

55

56

57

58

59

60

61

Plain Language Summary

The chemistry of fossil shells of planktic foraminifera, a type of marine zooplankton found throughout the global surface ocean, are commonly investigated to reconstruct past ocean and climate conditions. The chemistry of foraminiferal shells has been found to be reflective of the physical and chemical conditions of the water the shells grew within. However, biological processes can also affect shell chemistry, which may interfere with the way fossil shell chemistry is interpreted in past climate reconstructions. Here we investigate how planktic foraminiferal shell thickening or 'crusting', which occurs just after reproduction and just prior to death, could change the chemistry of a foraminiferal shell. To explore this question, the trace element and stable isotope shell chemistry was examined in populations of alive, fully mature, uncrusted specimens and recently deceased, crusted specimens collected from the same surface ocean

plankton tows. Results show that crusted shells tend to record lower trace element signatures then uncrusted shells, and investigation of trace element geochemistry within the shell wall shows that this is due to crusts having lower trace element concentrations. Changes to shell chemistry associated with crusting will need to be considered when establishing quantitative relationships between planktic foraminiferal shell chemistry and environmental conditions.

1. Introduction

75

76

77

78

79

80

81

82

83

84

85

86

87

88

89

90

91

92

93

94

95

96

97

98

99

100

101

102

103

104

105

Evaluation of trace element geochemistry, primarily trace element/Ca (TE/Ca) ratios such as Mg/Ca, of planktic foraminifera has become a cornerstone of paleoceanographic reconstructions (Katz et al., 2010; Allen et al., 2016). Although Mg/Ca of foraminifera has been well-studied as a sea surface temperature proxy (Nürnberg et al., 1996; Lea et al., 1999; Anand et al., 2003; Russell et al., 2004; Martínez-Botí et al., 2011, Hönisch et al. 2013), advances in technology and proxy understanding have led to greater investigation and utilization of other TE/Ca ratios (e.g., Ba/Ca, Mn/Ca, Na/Ca) to evaluate past ocean-climate change (Wit et al., 2013; Mezger et al., 2016; Davis et al., 2020; Watkins et al., 2021; Fritz-Endres et al., 2022). With the development of any new proxy in biological archives, it is necessary to not only constrain the primary environmental signal driving geochemical signatures, but also identify potential interference by vital effects, the biological impacts on shell geochemistry (Niebler et al., 1999; Schiebel and Hemleben, 2017). In general, fossil foraminiferal shells are an amalgamation of several stages of biotic, and in some cases abiotic, calcite growth (Hemleben et al., 1989; Branson et al., 2015). The biotic calcite stages include primary 'ontogenetic' calcite and, in some species, secondary 'gametogenic' calcite. Primary calcite is typically porous, exhibits pronounced laminations separated by organic layers, and for spinose species, acts as a base for spines to be supported (Branson et al., 2015). Many species of planktic foraminifera used in paleoreconstructions also add additional biotic calcite during or following reproduction and just prior to death, recognized as a 'gametogenic crust' (Fig. 1). This distinct gametogenic crust has long been identified as a feature of many planktic foraminiferal species (Bé and Lott, 1964; Bé, 1980; Caron et al. 1990). Lastly, an additional abiotic crust may be found in some fossil foraminifers that is attributed to post-depositional diagenetic processes occurring on the seafloor (Branson et al., 2015). Advancements in in-situ methodologies, such as laser-ablation inductively coupled plasma mass spectrometry (LA-ICP-MS), has allowed for greater insight into intrashell TE variability in foraminiferal shells as a means to investigate potential vital effects and relationships between different types of foraminiferal calcite (Eggins et al., 2003; Bolton and Marr, 2013; Steinhardt et al., 2015). LA-ICP-MS profiles from several different planktic foraminiferal species has shown that the gametogenic crust often yields lower TE/Ca values than the calcite grown throughout most of the foraminifers' early life in the surface ocean (i.e., the

early ontogenetic, or 'lamellar', calcite; **Table 1**). However, differences in TE/Ca between crust and early ontogenetic calcites are not found in all species nor is there a consistent crust 'signature' found within a given species (e.g., *Trilobatus sacculifer*; Eggins et al., 2003). Intrashell trace element investigations have focused primarily on Mg/Ca and thus our knowledge of intrashell variability of other TE/Ca proxies is limited (**Table 1**).

Similar investigations have delineated differences in isotopic composition between crusted and uncrusted foraminiferal shells (Vegnaud Grazzini, 1976; Blanc and Bé, 1981; Schweitzer and Lohmann, 1991; Mulitza et al., 1997; Bauch et al., 2002; Kozdon et al., 2009; Livsey et al., 2020). In several species, δ^{18} O values of crust calcite have been found to record higher values than the ontogenetic calcite, suggesting that the addition of gametogenic crust occurs deeper in the water column relative to the foraminifers living depth habitat (Duplessy et al., 1981). These isotopic differences have fueled hypotheses, which are still under debate (Meilland et al., 2021) surrounding reproductive strategies involving depth migration during gametogenesis (Hemleben et al., 1989; Schiebel and Hemleben, 2017).

Vital effects associated with foraminiferal ontogeny, and related differences in shell geochemistry, can have prolific consequences in paleoreconstructions if not properly considered. Many calibrations used to reconstruct past ocean conditions are derived from culturing studies whereby live foraminifera are collected from the surface ocean and brought back to the lab to be grown under controlled conditions. While culturing studies strictly constrain environmental controls on biogeochemical processes, they do not always well-simulate a foraminifer's natural habitat, and thus growth in culture is not always consistent with growth in nature. For example, shells grown in culture do not always develop a thick crust, even after gametogenesis when the crust is thought to form (Davis et al., 2017; Fehrenbacher et al., 2017). However, fossil foraminiferal shells used for paleoreconstructions typically display thick gametogenic crusts. Considering known geochemical differences between the crust and ontogenetic portions of crusted shells, it is possible that applying calibrations developed in the laboratory using noncrusted shells to crusted-shell fossil specimens may result in misleading paleoceanographic reconstructions. Here we further investigate this potential complication by comparing the trace element (Mg, Na, Ba, Sr, Mn, Zn) and stable isotope (δ^{13} C, δ^{18} O) composition of alive, fully mature, uncrusted (pregametogenic) shells to recently deceased, crusted shells of Neogloboquadrina pachyderma collected from the same discrete plankton tows. Because shells

were collected from the surface ocean, the "crusted" shells mentioned henceforth refer to shells composed of primary ontogenetic calcite and gametogenic crust, and do not include additional secondary diagenetic crust. Intrashell trace element variability is also examined in order to characterize geochemical differences between the crusted and ontogenetic portions of the shell wall. Lastly, stable isotope compositions of alive, uncrusted and dead, crusted populations are compared to stable isotope profiles of the water column measured from the same plankton tow collection sites to make inferences about where crusting occurs in the water column. By evaluating a species critical to paleoreconstructions at high latitudes, we aim to characterize the extent of geochemical differences between crusted and uncrusted shells, expand the analytes of interest beyond Mg/Ca (the focus of most studies— see **Table 1**), and explore the implications of such differences for paleoreconstruction.

2. Materials and Methods

2.1 Sampling

Neogloboquadrina pachyderma were collected from two stations along the Newport Hydrographic (NH) Line off the Oregon coast: NH85 (44.652°N, 126.050°W) and NH45 (44.652°N, 125.117°W) in May 2022 (**Fig. 2**). *N. pachyderma* are an asymbiotic, non-spinose taxon found abundantly in the study region when cooler waters are present (Ortiz and Mix, 1992; Takagi et al., 2019; Lane et al., 2023), and they serve as an important species to reconstruct polar to subpolar paleoceanographic conditions. A 150 µm plankton tow net was used to sample the uppermost 200 m of the water column, sampled as two continuous tows from 200 m depth to the surface. While N. pachyderma have been found at greater depth habitats in other regions (i.e., Greco et al., 2019), the sampling was constrained to the upper 200 m of the water column to ensure that we were sampling populations calcifying from the same water depth and that geochemical differences between alive, uncrusted and dead, crusted could be directly attributed to the process of gametogenic crust development as opposed to any additional geochemical changes associated with the shells sinking through the water column (e.g., scavenging). Previous depth stratified tows conducted in the study region (Ortiz et al., 1996) have found minor concentrations (<0.25 individuals/m³) of N. pachyderma below 200 m water depth. Fully-mature, live specimens and recently deceased, crusted specimens of N. pachyderma were immediately wet picked from each tow, rinsed with distilled water, and placed in micropaleontological slides.

Alive specimens were identified by their distinctive brightly colored cytoplasm and relatively thin shell walls, whereas the shells of recently deceased foraminifers were free of cytoplasm, appeared white under reflective light, and exhibited a thick crust (**Fig. 1**). A total of 66 dead shells (NH85: N=52; NH45: N=14) and 55 alive shells (NH85: N=44; NH45: N=11) were collected.

Conductivity-temperature-depth (CTD) profilers were used to characterize the water column at each site and showed consistent conditions at NH85 and NH45 (**Fig. 3**), supporting the pooling together of samples from both sites. Seawater samples were collected from both study sites from the following depths: 5 m, 2 5m, 50 m, 100 m, 150 m, 250 m, and 500 m, to establish stable isotope profiles. Seawater samples collected for δ^{13} C analysis of the dissolved inorganic carbon were poisoned with mercuric chloride (HgCl₂) immediately upon collection. Seawater samples obtained for δ^{18} O analysis were collected in scintillation vials and capped with a positive meniscus at the top of each vial to avoid atmospheric exchange post-collection.

2.2 LA-ICP-MS TE/Ca analysis

2.2.1 Sample preparation

Prior to geochemical analyses, specimens were rinsed and oxidatively cleaned to remove remnant organic matter, following previously established protocols, adapted for single shells (Martin and Lea, 2002). To remove any detritus, the shells were rinsed with ultrapure (milliQ) water, followed by methanol, and then given an additional rinse with ultrapure water. Next, shells were submerged in a 1:1 solution of 30% H₂O₂ buffered with 0.1 M NaOH, and vials were placed in a hot (65°C) water bath for 10 minutes. The solution was removed from the sample vials, and shells were rinsed three times in ultrapure water. Shells were subsequently mounted on a slide covered with strips of carbon tape in preparation for in-situ trace element analysis.

2.2.2 LA-ICP-MS Analytical Methods

All specimens were analyzed via LA-ICP-MS to evaluate trace element geochemistry. Shells were analyzed using a Thermo Scientific iCAP RQ inductively coupled plasma mass spectrometer coupled to an Applied Spectra RESOlution laser ablation system in the Keck Collaboratory for Plasma Spectrometry at Oregon State University. Ten isotopes were measured with the following seven isotopes evaluated herein: ²³Na, ²⁴Mg, ⁴³Ca, ⁵⁵Mn, ⁶⁶Zn, ⁸⁸Sr, and ¹³⁸Ba.

Isotopes were measured using a rapid peak-hopping procedure with the following dwell times for each isotope: 23 Na = 0.04 s, 24 Mg = 0.02 s, 43 Ca = 0.01 s, 55 Mn = 0.05 s, 66 Zn = 0.05 s, 88 Sr = 0.02 s, and 138 Ba = 0.05 s. Shells were ablated from the outer shell surface through to the interior of the shell at a repetition rate of 5 Hz and a laser energy of 4.0 mJ attenuated by 75% to 87.5%, focused upon 24 - 38 µm spot sizes. The last four chambers in the final whorl, F₀ (ultimate chamber) to F₃ (Fig. 1d), were analyzed with repeated analysis on at least one chamber per specimen to assess reproducibility (Table S1). Shell averages reported herein were calculated by first averaging repeated analyses on single chambers, followed by equal-weight averaging of the chamber averages. In <6% of the specimens, the F3 chamber was too small or not accessible due to the orientation of the specimen on the tape, and thus was not analyzed or included in the calculation of the whole-shell value. Analysis of shells was periodically bracketed by analysis of three standard reference materials (SRM): NIST glasses 610 and 612, and the USGS standard MACS-3. Each standard was ablated for 60 s at an energy of 5.00 mJ using a 50 µm spot size. All element concentrations were determined using NIST 610 and NIST 612, however due to consistent Na concentrations found in NIST glasses, Na was evaluated using the NIST 610 and MACS-3 SRMs. Elemental calibrations of SRMs measured throughout the analysis session yielded $r^2 \ge 0.99$.

2.2.3 Data Analysis Methods

LA-ICP-MS data was processed using the Python package LA-Tools (Branson et al., 2019) which follows established data reduction protocols (Longerich et al., 1996). Data processing protocols include despiking and signal smoothing to remove outliers, evaluating and applying any necessary drift correction using the bracketing SRM analyses, and removing average background counts from each data point. The mean TE/Ca for each profile (i.e., individual chamber analysis) is then calculated by normalizing to the known trace element concentrations of the drift-corrected SRM standards (Jochum et al., 2011).

Several approaches were employed to investigate differences between whole-shell, intrashell, and chamber-to-chamber variability. The distributions of whole-shell and individual chamber (i.e., F0, F1, F2, F3; **Fig. 1d**) TE/Ca values were compared between the uncrusted (alive upon collection) and crusted (dead) shells. A Shapiro-Wilks test determined that nearly every population was non-normally distributed, and thus a Mann-Whitney test was used to

evaluate if the uncrusted versus crusted trace element chemistries were statistically significantly different (denoted by a red star in Fig. 4).

The intrashell depth profiles are used to explore intrashell TE variability and reflect changes in trace element geochemistry as the laser ablated from the outside of the shell through the shell wall (e.g., Fig. 5). To aid in the interpretation of the intrashell geochemical variability on a population scale, the TE/Ca data from the depth profiles were plotted on a 1:1 plot, where the average of the outer 50% of the data from each individual depth profile (reflecting mostly crust calcite, if present) was plotted against the inner 50% average of data obtained from the same specimen (reflective of the ontogenetic calcite) (Fig. S1, S2). The difference in TE/Ca between the inner 50% and outer 50% of each depth profile (ΔTE/Ca_{inner-outer}) was calculated and plotted relative to a zero line (Fig. 6). If the inner, ontogenetic calcite is more enriched in a given TE, the difference will plot above the zero line in Figure 6 (above the 1:1 line in Figures S1 and S2). If the outer, crust calcite yields higher TE concentrations, the inner-outer difference will plot below the zero line in Figure 6 (below the 1:1 line in Figures S1 and S2). If there are no distinct differences in the concentration of a given TE between the inner and outer calcites, values will plot near or on the zero line in **Figure 6** (on or near the 1:1 line in **Figures S1 and S2**). The distributions for whole shell values for the alive, uncrusted shells are compared to the distributions of the inner 50% spectral averages and outer 50% spectral averages of the dead crusted shells (Fig. 7). Inner 50% chamber spectral averages, outer 50% chamber spectral averages, and TE/Ca shell averages can be found in Supplemental Datasets S1 through S6, for Mg/Ca, Na/Ca, Sr/Ca, Ba/Ca, Mn/Ca, and Zn/Ca, respectively.

250251

252

253

254

255

256

257

258

259

260

230

231

232

233

234

235

236

237

238

239

240

241

242

243

244

245

246

247

248

249

2.3 Stable Isotope (δ^{13} C & δ^{18} O) Analysis

2.3.1 Stable Isotope (δ^{13} C & δ^{18} O) Analysis of Foraminiferal Shells

Study specimens were analyzed for stable carbon (δ^{13} C) and oxygen (δ^{18} O) isotopes following completion of LA-ICP-MS analysis. Stable isotope measurements were performed at the Oregon State University Stable Isotope Laboratory using a Thermo Scientific Kiel IV carbonate device interfaced to a Thermo Scientific MAT 253 dual-inlet gas-source isotope ratio mass spectrometer. Two to three foraminiferal shells of the same life stage (dead vs. live) were pooled together for each individual stable isotope analysis due to low masses. In total, 23 separate analyses of dead foraminifera and 19 separate analyses of shells of alive specimens were

conducted. Replicate analyses of NBS19 (δ^{13} C = 1.95‰ VPDB, δ^{18} O = -2.2‰ VPDB) and inhouse standard CaCO₃ standard "Wiley" (δ^{13} C = -0.41‰ VPDB, δ^{18} O = -7.20‰ VPDB) resulted in an analytical precision (1SD) of \leq 0.05‰ and \leq 0.08‰ for δ^{13} C and δ^{18} O, respectively. All shell stable isotope data can be found in **Supplementary Dataset S7**.

2.3.2 Stable Isotope Analysis of Dissolved Inorganic Carbon ($\delta^{13}C_{DIC})$ and Seawater ($\delta^{18}O_{sw})$

Seawater samples were collected from the two study sites for comparison between the isotope signatures recorded by the shells and isotope profiles of the water column (**Figs. 8, 9**). Seawater samples were analyzed in the Stable Isotope Laboratory at Oregon State University. The carbon isotope analysis of the dissolved organic carbon of seawater ($\delta^{13}C_{DIC}$) was analyzed using a Thermo Scientific Delta V isotope ratio mass spectrometer fitted to a gas bench. For each sample 1 mL of seawater was injected into a sealed, helium-flushed vial. Prior to analysis, 100 μ L of 85% H₃PO₄ were injected into the sample vial and left to equilibrate for 8 hours. Two standards were analyzed over the course of each run to check stability and calibrate reference gases: an in-house Wiley standard and 0.7 mL of 3mM NaHCO₃. Repeated analysis of standards resulted in an analytical error (standard deviation) for δ^{13} C of $\pm 0.03\%$. All $\delta^{13}C_{DIC}$ data are reported relative to VPDB (**Fig. 8**; **Table 2**).

Oxygen isotope analysis of seawater ($\delta^{18}O_{sw}$) samples were conducted using a Thermo Scientific Delta PlusXL mass spectrometer with a water equilibration system. Seawater samples were calibrated using three internal standards ("LROSS-6", $\delta^{18}O = -10.97\%$; "HOT-4", $\delta^{18}O = -0.17\%$; "Seawater", $\delta^{18}O = -0.55\%$) scattered throughout and bracketing each run. The isotopic compositions of LROSS-6 and HOT-4 internal standards have been calibrated using the international standards VSMOW, GISP, and SLAP. Samples were analyzed using the CO₂ equilibration method and dual inlet isotope ratio mass spectrometry, with an analytical error (standard deviation of repeated standard runs) of $\pm 0.05\%$. All $\delta^{18}O_{sw}$ data are reported relative to VSMOW in **Table 2**. The predicted $\delta^{18}O$ for calcite precipitated at equilibrium from seawater ($\delta^{18}O_{calcite}$) was calculated for comparison to the $\delta^{18}O$ values of the foraminiferal shells. The predicted $\delta^{18}O_{calcite}$ value for each water depth (**Table 2**) was calculated using the seawater temperature (from the CTD cast), the measured $\delta^{18}O_{sw}$ values, and the following precipitation equilibrium equation from Kim and O'Neil (1997):

 $1000 \ln \alpha_{\text{(Calcite - H2O)}} = 18.03(10^{3}T^{-1}) - 32.42$ (Eq. 1)

where T is in kelvin and α is the fractionation factor. Values produced by Eq. 1 are determined relative to the VSMOW scale, and were subsequently converted to the PDB scale for direct comparison to the measured $\delta^{18}O_{FORAM}$ values using the following equation from Coplen et al. (1983):

297
$$\delta^{18}O(\% PDB) = 0.97002 \times \delta^{18}O(\% VSMOW) - 29.98$$
 (Eq. 2)

Most paleoceanographic studies utilizing *N. pachyderma* use either the Kim and O'Neil (1997) or O'Neil (1969) equations (Kozdon et al., 2009), thus the Kim and O'Neil (1997) equation was employed to reconstruct predicted equilibrium calcite oxygen isotope values shown herein.

3. Results

3.1 Whole-Shell and Individual Chamber TE Differences

Mg/Ca values were similar in the crusted and uncrusted shells, both in their whole shell and individual chamber distributions (**Fig. 4a**). Zn/Ca ratios also displayed overlapping distributions between the two populations, however the distributions of values for the uncrusted shells were skewed to higher values than the distributions derived from the crusted shells (**Fig. 4f**). Only Zn/Ca values from the F3 chamber were found to be significantly different between the crusted and uncrusted populations.

The four remaining elemental ratios, Ba/Ca, Na/Ca, Mn/Ca, and Sr/Ca, all show distinct differences between the crusted and uncrusted shells. The uncrusted shells record significantly higher TE/Ca compositions compared to the crusted shells (**Fig. 4**). When observing TE/Ca differences in individual chambers, significant differences between the crusted and uncrusted shells are also found, however these differences tend to increase in sequentially older chambers. For example, the Sr/Ca difference between the uncrusted and crusted population means increase from 0.011 mmol/mol to 0.031 mmol/mol to 0.075 mmol/mol to 0.080 mmol/mol for the F0, F1, F2, and F3 chambers, respectively (**Fig. 4e**). A similar increase is observed in Ba/Ca, Na/Ca, and Mn/Ca. All Ba/Ca (**Fig. 4b**) and Na/Ca (**Fig. 4c**) chamber populations were statistically different between the crusted and uncrusted shells. The F1, F2, and F3 chambers recorded significant differences in Sr/Ca, and the F2 and F3 chambers recorded significant differences in Mn/Ca. Statistically significant differences were determined using a Mann-Whitney test (p-values < 0.05) and are marked with an asterisk (**Fig. 4**).

323324

325

326

327

328

329

330

331

332

333

334

335

336

337

338

339

340

341

342

343

344

345

346

347

348

349

350

351

352

353

3.2 Intrashell Trace Element Variability

Distributions of $\Delta TE/Ca_{inner-outer}$ values (where $\Delta TE/Ca_{inner-outer} = Avg(TE/Ca)_{inner50\%}$ - $Avg(TE/Ca)_{outer50\%}$) provide insight into how the crusted and uncrusted intrashell geochemistry differ on three fronts: 1) $\Delta TE/Ca_{inner-outer}$ show if a portion (i.e., inner 50% or outer 50%) of the shell wall is more enriched in a TE compared to the remainder of the shell wall, 2) the magnitude of TE enrichment within a portion of the shell wall as identified by distributions of $\Delta TE/Ca_{inner-outer}$ values can be compared between crusted and uncrusted populations, and 3) the chamber-to-chamber variability in $\Delta TE/Ca_{inner-outer}$ values can be examined. Here we will review each of these results for the examined analytes. Differences between distributions will be described primarily via a comparison of the innermost quartile ranges.

Differences in Mg/Ca between the inner and outer calcite (ΔMg/Ca_{inner-outer)} tend to be minimal for the uncrusted shells, as indicated by the overlap of $\Delta TE/Ca_{inner-outer}$ distributions with the line of equality or "0" line. In contrast, the crusted shells consistently have positive AMg/Cainner-outer values that increase in progressively older chambers (Fig. 6a). Both the crusted and uncrusted N. pachyderma shells have enriched Ba/Ca values in the inner calcite, though the $\Delta Ba/Ca_{inner-outer}$ values tend to deviate farther from the line of equality in crusted shells (**Fig. 6b**). Nearly all chambers show higher Na/Ca in the inner chamber calcite in both crusted and uncrusted shells, as proven by the distinctly positive $\Delta TE/Ca_{inner-outer}$ distributions (**Fig. 6c**). Only the F0 chamber in the uncrusted shells lacks a $\Delta Na/Ca_{inner-outer}$ difference. The $\Delta Na/Ca_{inner-outer}$ values increases markedly in sequentially older chambers. There is only a slight $\Delta Mn/Ca_{inner-outer}$ difference in uncrusted shells (Fig. 6d). Conversely, crusted shells have a positive ΔMn/Ca_{inner-} outer difference in all chambers. The $\Delta Sr/Ca_{inner-outer}$ values show chamber-to-chamber patterns like those observed with Na/Ca, where ΔSr/Ca_{inner-outer} values increase in progressively older chambers in both the crusted and uncrusted shells (Fig. 6c, e). However, differences in the distribution of Δ Sr/Ca_{inner-outer} values between the youngest (F0) and oldest (F3) chambers is greater among the alive, uncrusted shells when compared to the crusted shells. The F0 and F1 chambers of the uncrusted shells tend to record similar Sr/Ca in the inner and outer halves of the shell wall, whereas the F2 and F3 chambers tend to record higher Sr/Ca in the inner chamber wall. Crusted shells show slight Sr/Ca enrichment in the outer calcite in the F0 chamber and Sr/Ca enrichment in the inner calcite in the F1, F2, and F3 chambers. Zn/Ca is higher in the inner shell wall of both crusted and uncrusted shells, however crusted shells record consistently more positive $\Delta Zn/Ca_{inner-outer}$ values than their uncrusted counterparts (**Fig. 6f**). Chamber-to-chamber variability in Zn/Ca is minimal.

The inner 50% of the crusted specimens, primarily composed of early ontogenetic calcite, should be most similar in composition to the uncrusted specimens, which are composed of only early ontogenetic calcite, with little or no crust calcite. A comparison of uncrusted whole-shell TE/Ca data to the TE/Ca data from the inner 50% of the crusted shells demonstrates this similarity (**Fig. 7**). For most TEs the TE/Ca distributions of the inner 50% of the crusted shells are statistically similar to the TE/Ca distributions of the uncrusted, whole-shell values. Conversely, the outer 50% of the dead, crusted shells are significantly different than the alive, uncrusted shells, recording consistently lower TE concentrations. Only in the case of Sr/Ca are both the crusted inner 50% and outer 50% values significantly different than the uncrusted, whole shell values (**Fig. 7c**).

3.3 Stable isotope ($\delta^{13}C$ and $\delta^{18}O$) differences between crusted and uncrusted shell populations

Uncrusted shells generally record higher carbon isotope values and lower oxygen isotope values compared to the crusted shells retrieved from the surface ocean environment (**Fig. 8**). Carbon isotope values for the alive, uncrusted shells range from 0.63‰ to -0.07‰ with an average value of 0.25‰ whereas δ^{13} C values for the dead, crusted shells range from 0.29‰ to -0.28‰ with an average of -0.05‰ (**Fig. 8a**). Oxygen isotope values range from 0.56‰ to -0.14‰ for uncrusted shells, with an average of 0.12‰, and values range from 0.89‰ to 0.06‰ for crusted shells, with an average of 0.37‰ (**Fig. 8b**). Differences in isotopic composition between the crusted and uncrusted shells are statistically significant for both δ^{13} C and δ^{18} O (Student's t-test; δ^{13} C, p-value <<0.001).

4. Discussion

4.1 Trace element variability in crusted and uncrusted specimens

The whole shell average Ba/Ca, Na/Ca, Mn/Ca, and Sr/Ca are significantly higher in the uncrusted shells of *N. pachyderma* compared to crusted shells recovered from the same surface-ocean plankton tows (**Fig. 4b-4e**). Inner calcite TE enrichment (i.e., more positive ΔTE/Ca_{inner}-

outer) is present in both crusted and uncrusted shells but is more pronounced in the crusted specimens (**Fig. 6**). Mg/Ca and Zn/Ca are not significantly different in the uncrusted versus crusted specimens, but the range of values recorded in uncrusted shells is skewed toward higher ratios compared to the crusted shells (**Fig. 4a, f**). Comparison of the outer 50% spectral averages (i.e., dominantly crust calcite) to whole-shell uncrusted TE values show a significant TE depletion in the crust calcite (**Fig. 7**). Thus, differences in whole-shell trace element geochemistry, and the positive $\Delta TE/Ca_{inner-outer}$ values, are attributed to the low TE-bearing crust calcite, which lowers the overall whole-shell average TE/Ca ratios (**Fig. 6**). The crust, which tends to grow thicker on the progressively older chambers, is also likely responsible for the larger $\Delta TE/Ca_{inner-outer}$ differences in progressively older chambers (e.g., **Fig. 4b-e; Fig. 6**; Sadekov et al. 2005, Fehrenbacher et al., 2017).

High-resolution analyses from fossil specimens demonstrate that nearly all TEs in early ontogenetic calcite are elevated compared to crusted calcite whereas the outer crust is generally more homogeneous, with overall lower trace element ratios (Sadekov et al., 2005; Hathorne et al., 2009; Steinhardt et al., 2015; Jonkers et al., 2016; **Table 1**). The ontogenetic TE-enriched calcite often appears 'banded', with alternating high and low intercalated calcite 'layers' (Sadekov et al., 2005; Hathorne et al., 2009; Steinhardt et al., 2015; Bonnin et al., 2019). The higher ratios of these elements in the innermost chamber walls could be related to the presence of organic layers embedded in the shell wall that form with chamber growth and thickening processes. Chamber formation processes are variable amongst different species but share a common feature: as the chambers are added and/or thickened during early ontogeny, organic membranes form between the thin calcite layers. The initial calcite that forms adjacent to the organic membrane is often enriched in TEs (Cuif et al., 2012; Fehrenbacher et al., 2017; Bonnin et al., 2019, Richey et al., 2022). The mechanism responsible for the enriched TEs associated with the organic membranes is poorly constrained but may be linked to processes responsible for nucleating calcite on the organic templates (Branson et al., 2019).

The higher ratios in the inner calcite could also reflect variable conditions in the microhabitat surrounding the shells during early ontogeny. The microhabitat is a complicated space that has remarkably different chemistry compared to the adjacent seawater (Jørgensen et al., 1985; Rink et al., 1998). First, foraminifera respire, which likely modulates the carbonate chemistry and oxygen concentration in the microenvironment around their shells. Studies have

also demonstrated that foraminifera increase the pH in the microenvironment during chamber formation (de Nooijer et al., 2008, 2009). For species with algal symbionts, the changes in pH and oxygen are even more pronounced due to diurnal algal photosynthesis cycles (Jørgensen et al., 1985; Kohler-Rink et al., 2000). While our study species is asymbiotic and thus is not affected by photosynthetic cycles, there is growing evidence that non-spinose foraminifera, including N. pachyderma, calcify within a particulate organic microhabitat, such as marine snow, during early ontogeny (Fehrenbacher et al., 2018; Greco et al., 2019; Fritz-Endres et al., 2022; Richey et al., 2022). Marine snow can have highly variable pH, oxygen concentrations, and even different seawater trace element compositions (Hebel et al., 1986; Alldredge and Cohen, 1987). During periods of high productivity, calcification within marine snow can be more common, resulting in higher Ba/Ca ratios among non-spinose foraminifera (Fritz Endres et al., 2022). However, the specimens examined in this study were captured during a period of relatively low productivity (i.e., chlorophyll a < 0.25 mg/m³; Fig. 3) and so we do not find high Ba/Ca compositions like those observed in other studies of non-spinose foraminifera (Fehrenbacher et al., 2017; Richey et al., 2022). Although the exact mechanism responsible for differences in the geochemistry of the early ontogenetic calcite and the outer crust is not well constrained, results herein confirm that the inner calcite of N. pachyderma has consistently enriched TEs whereas the crust calcite consistently records lower trace elements (Fig. 4, 6, 7).

Crust formation remains an enigmatic process (Hamilton et al., 2008). Why are trace elements lower in crust calcite when compared to the early ontogenetic calcite? Moreover, why does the crust lack TE variability? Although it is widely accepted that foraminifera crusting occurs during late ontogeny, and typically during or just prior to gametogenesis, the mechanisms modulating TE incorporation during this process are not well constrained. In the foraminiferal species *Orbulina universa* and *N. dutertrei*, it has been shown that calcite that forms during the day has lower Mg/Ca ratios compared to calcite that forms at night. If the crust forms rapidly, and during daylight hours, this may be responsible for the low TE composition of the crust calcite (Spero et al., 2015; Fehrenbacher et al., 2017). Culture studies using foraminiferal species that have been shown to generate crust in culture, like *N. incompta* (Davis et al., 2017), could shed further light on TE incorporation processes during crusting.

Intrashell variability was evaluated by examining chamber-to-chamber variability and $\Delta TE/Ca_{inner-outer}$ gradients. $\Delta TE/Ca_{inner-outer}$ gradients were used to determine if the outer crusted

calcite recorded relatively lower TE concentrations. While this is a useful tactic to evaluate the general chemical distribution in the crust versus ontogenetic calcite on a population scale, it inherently simplifies the structure of TE variability in the shell wall. For example, in **Figure 5a**, Zn/Ca is consistently low in the outer 50% of the spectrum whereas it increases to a distinct peak in the inner 50% of the spectrum. The general structure of Zn/Ca observed in **Figure 5a** supports an idealized view of a "low TE" crust that appears to be clearly distinguishable from the inner ontogenetic calcite. However, Ba/Ca of the same shell (**Fig. 5b**) shows several bands of fluctuating high and low Ba/Ca throughout the entire spectrum, although when calculated the average of the inner 50% of the spectrum is higher than the average of the outer 50%. While these observations do not hinder the interpretations described herein, it is worth noting that intrashell TE variability is simply more complex than the ΔTE/Ca_{inner-outer} gradients that were employed to assess it. However, comparison of representative TE/Ca spectra from a crusted specimen and an uncrusted specimen (**Fig. 5**) shows that greater variability is found throughout the depth profile in uncrusted specimens, whereas inner-outer TE differences are generally more visually apparent in crusted specimens.

4.2 Habitat depth and crust formation: insights from stable isotopes

While the planktic foraminiferal life-cycle and preferred habitat depth is an ongoing area of research (e.g., Meilland et al., 2021), it is generally believed that many species of foraminifera undergo gametogenesis and grow the associated crust at depths deeper than their typical, average, living depth habitat (Duplessy et al., 1981; Hemleben et al., 1989; Bauch et al., 2002; Schiebel and Hemleben, 2017). Stable isotope data from the crusted and uncrusted shell populations presented herein support this notion. The uncrusted shells record higher δ^{13} C values and lower δ^{18} O values compared to crusted shells acquired from the same plankton tow (**Fig. 8**). These differences suggest that *N. pachyderma* live in the 13 C-enriched, warmer waters of the upper surface ocean during early ontogeny and develop the late gametogenic crust deeper in the water column. The relatively cooler temperatures are responsible for the higher δ^{18} O signature of the crusted specimens while the increase in organic matter decomposition in deeper water lowers the seawater δ^{13} C_{DIC}, thereby also lowering the δ^{13} C_{FORAM} (i.e., shell) composition. Similar relative differences have been found in isotopic comparisons of crusted and uncrusted shells of both spinose (Vegnaud Grazzini, 1976; Blanc and Bé, 1981; Schweitzer and Lohmann, 1991;

Mulitza et al., 1997) and non-spinose (Bauch et al., 2002; Kozdon et al., 2009; Livsey et al., 2020) species.

478

479

480

481

482

483

484

485

486

487

488

489

490

491

492

493

494

495

496

497

498

499

500

501

502

503

504

505

506

507

508

The δ^{13} C values recorded by both crusted and uncrusted shells are within the range of $\delta^{13}C_{DIC}$ values measured from the upper water column, suggesting that the N. pachyderma examined herein were collected during a low productivity period and grew their shells in equilibrium with seawater $\delta^{13}C_{DIC}$. A similar observation is made when comparing the $\delta^{18}O_{FORAM}$ population distribution to the $\delta^{18}O$ profile of predicted equilibrium calcite (Fig. 8, 9). We therefore argue that comparisons between shell and water isotope geochemistry can be used to make inferences about the living depth habitat and depth of crusting (Fig. 9). The uncrusted $\delta^{13}C_{FORAM}$ values suggest that these foraminifer calcified between ~45 to 85 m below the surface during their lifetime. The distribution of the crusted shells aligns with $\delta^{13}C_{DIC}$ signatures found at depths of ~73 to 102 m. However, crusted shells are a mixture of ontogenetic calcite and crust calcite. If we assume that the average δ^{13} C value of the living shell distribution is representative of the ontogenetic calcite shell ($\delta^{13}C_{onto} = 0.24\%$) and use the average $\delta^{13}C$ value of the crusted shells as our 'mixed' signature ($\delta^{13}C_{\text{crusted}} = -0.05\%$), we can determine potential crusting depths by modeling various scenarios of % crust and % ontogenetic calcite (Fig. 9a). For example, if the crusted shells were a mixture of 70% crust calcite and 30% ontogenetic calcite, the crust calcite would need to have been added at a depth of \sim 92 m where the $\delta^{13}C_{DIC}$ is -0.17‰, Conversely, if crusted shells were composed of 40% crust calcite and 60% ontogenetic calcite, the crust would need to be added at near a depth of ~227 m where the $\delta^{13}C_{DIC}$ is -0.49‰. A 30% crust calcite/70% ontogenetic calcite mixture would require the crust calcite end-member to have a δ^{13} C signature of -0.73% which is below the minimum δ^{13} C_{DIC} values recorded in the upper 500 m of the water column. These mixing scenarios, in combination with the fact that all shells were collected from the uppermost 200 m of the water column, suggest that shells are composed of between 40-70% crust calcite, and that crusting likely occurs between ~100 and 200 m below the surface. Estimates of crust volume interpreted here are consistent with SEM imaging of shell cross sections and mass-balance calculations derived from weight comparisons of crusted and uncrusted shells where the crust calcite has been found to compose anywhere from ~30 to 70% of the total shell volume (Bé, 1980; Mulitza et al., 1997; Bauch et al., 2002; Bolton and Marr, 2013). The depth of crusting determined herein is also consistent with observations of N. pachyderma from plankton tow studies in the Okhotsk Sea (Bauch et al.,

2002) but is shallower then crusting depths found in the Labrador Sea, Greenland Sea, and Fram Strait (~200 to 400 m; Stangeew, 2001, Kozdon et al., 2009). Studies of *N. pachyderma* populations throughout the Arctic have found depth habitats (calculated as the abundance-weighted mean depth determined using the midpoints of the collection intervals) ranging from 25 to 280 m water depth (Greco et al., 2019). Sparse depth-stratified assemblage data published for the study region (Ortiz et al., 1996) have found specimens living dominantly within the upper 200 m of the water column, with shells found below 200 m representing a settling flux of dead shells. The variable depth at which crust forms is likely driven simply by hydrographic conditions, which will differ across study regions.

Comparisons of the $\delta^{18}O_{FORAM}$ range to the $\delta^{18}O$ profile predicted from calcification at equilibrium with seawater produces an estimated living depth habitat of ~30 to 68 m. If we employ a similar mixing model approach using the average $\delta^{18}O$ of the uncrusted shells ($\delta^{18}O_{onto}$ = 0.08‰) as the ontogenetic calcite end-member and the average $\delta^{18}O$ of the crusted shells as the "mixed" signature, crusting mixtures of $\geq 20\%$ provide reasonable crusting depths near or within the uppermost 200 m of the water column.

While the δ^{13} C mixing model provides a first approximation of crusting depths, it is possible that the foraminiferal calcite may not be directly recording the δ^{13} C_{DIC}. Isotopic investigations of *N. pachyderma* from the Okhotsk Sea have recognized offsets between δ^{13} C_{DIC} and δ^{13} C_{shell} that were attributed to grow under lower carbonate ion concentrations (i.e., the "carbonate ion effect" (Spero et al., 1997; Bauch et al., 2002). However, consistency in the interpreted living depth habitats interpolated from both the δ^{13} C and δ^{18} O shell distributions provides some confidence that the foraminiferal δ^{13} C is not strongly affected by carbonate ion concentration in our study region.

4.3 Crusting in planktic foraminifera: implications for paleoreconstruction

Intrashell TE variability has been widely explored in many planktic foraminiferal species using an array of techniques including LA-ICP-MS and electron microprobe mapping, among others (**Table 1** and references therein). Together, this body of literature suggests that for most planktic foraminiferal taxa the crust portions of foraminiferal shells tend to record lower trace elements, leading to overall lower whole-shell trace element concentrations in crusted shells. These previous studies have generally focused on Mg/Ca variability and evaluations derived

from a few individuals. Here, we expand the investigated elements and work to constrain patterns observed consistently in a larger population to better understand trace element incorporation for a single, critically important foraminiferal species. Population-scale geochemical TE/Ca variability, statistically-robust evaluations of intrashell variability, and associated differences between crusted and uncrusted shell populations collected from the same plankton tows in the upper surface ocean demonstrate how shell geochemistry changes in association with gametogenic crust formation. Results serve as a baseline for comparison to regional sediment trap and core-top studies to better delineate geochemical changes that occur between initial calcification in the water column and fossilization on the seafloor.

540

541

542

543

544

545

546

547

548

549

550

551

552

553

554

555

556

557

558

559

560

561

562

563

564

565

566

567

568

569

A few observations presented herein deviate from precursor studies. While Mg/Ca has been found to generally be lower in crust calcite when compared to ontogenetic calcite for most taxa (Table 1), we do not find significant differences when comparing Mg/Ca values derived from uncrusted and crusted shells of N. pachyderma (Fig. 4a, 6a). Significant differences in Mg/Ca are found when comparing the outer 50% of the crusted shells to the uncrusted wholeshell values (Fig. 7a), but the translation of these differences into whole-shell values does not appear to produce a vital effect that would affect temperature estimates derived from these shells. The small differences in Mg/Ca between the crust and ontogenetic portions of the shells may be supportive of either 1) interpretation that these shells are minimally crusted or conversely, 2) that crusting is occurring over a small temperature gradient between living depth and crusting depth. Specimens that calcify when there is a larger temperature gradient over the depth habitat range may have larger Mg/Ca differences in ontogenetic versus crust calcite. It has also been argued that the depth of crusting varies for a foraminifer following gametogenesis, as interpreted by chamber-to-chamber differences observed in Mg/Ca in studies of N. dutertrei (Jonkers et al., 2012). Yet TE/Ca content in crusted specimens of N. pachyderma examined in this study record very similar Mg/Ca distributions in the penultimate and preceding chambers (i.e., F1 to F3 chambers; Fig. 4) suggesting rapid crust development occurring at a consistent depth. Although we do not find distinct differences in Mg/Ca between crusted and uncrusted individuals collected via plankton tow, there is a potential for Mg/Ca alteration of shells to occur while settling through the water column and/or upon deposition to the seafloor (Dekens et al., 2002; Sadekov et al., 2010; Wycech et al., 2016). Precipitation of secondary diagenetic calcite at lower

temperatures, such as those found along the seafloor, would further increase the relative volume of low-Mg calcite in the shells of fossil foraminifers.

There is growing interest in understanding mechanisms responsible for the incorporation of the elements Na, Mn, Zn, and Ba, because of their potential utility in paleoclimate as proxies for salinity, oxygenation, water mass tracing, and paleoproductivity, respectively (Marchitto et al., 2000; Bryan and Marchitto, 2010; Wit et al., 2013; Steinhardt et al., 2014; Mezger et al., 2016; Bertlich et al., 2018; Fehrenbacher et al., 2018; Watkins et al., 2021; Fritz-Endres et al., 2022). For *N. pachyderma*, results herein demonstrate that these elements are highly variable in the early ontogenetic calcite and that the crust calcite has overall lower TE/Ca ratios. Culture experiments remain invaluable for understanding mechanisms responsible for the incorporation of these elements. However, for species that form crusts, crusted plankton tow, sediment trap, and seafloor specimens may be better suited for the generation of TE-environment calibrations that can be applied to downcore reconstructions. Depending on the region, crusted shells are more likely to be preserved in the fossil record (Caron et al., 1990; Johnstone et al., 2010), and thus in these cases, calibrations to appropriately assess their geochemistry should be prioritized.

5. Conclusions

Culturing studies of foraminifera have been invaluable to the field of paleoceanographic proxy development (Schiebel and Hemleben, 2017), however culturing of planktic foraminifera is not without its hardships. Previous culturing studies of neogloboquadrinids have noted difficulty in getting foraminifera to develop thick crusts similar to those found in nature (Davis et al., 2017; Fehrenbacher et al., 2017). Here we examine trace element (Mg/Ca, Na/Ca, Sr/Ca, Ba/Ca, Mn/Ca, Zn/Ca) and stable isotope (δ¹³C, δ¹8O) geochemistry of crusted and uncrusted shells of *Neogloboquadrina pachyderma* collected from the same surface ocean plankton tows to investigate potential vital effects associated with the development of gametogenic crusts. Results herein show that for most TEs (Na, Sr, Ba, Mn), TE/Ca values are significantly higher in uncrusted shells when compared to crusted shells. Whole-shell TE values are lower for crusted shells due to the inclusion of low TE-bearing crust. Stable isotope comparisons of foraminiferal shells to ambient seawater indicate that *N. pachyderma* live within the uppermost 90 m of the water column. We have estimated that the crust composes ~40 to 70% of the shell volume in crusted shells, and that crusting occurs between ~100 to 200 m water depth. If TE/Ca culture

001	calibrations are established from 1E-enriched uncrusted or weakly-crusted shells and applied to
502	crusted fossil shells, the associated paleoreconstructions will inherently produce attenuated
503	climate signals. We therefore recommend 1) using calibrations established from crusted
504	specimens to evaluate fossil records; or 2) that calibrations based on ontogenetic calcite should
505	be only applied to the ontogenetic portions of fossil specimens using LA-ICP-MS profiling, as
506	previously suggested by Davis et al., (2017).
507	
808	Acknowledgements
509	This research is supported by the NOAA Climate and Global Change Postdoctoral Fellowship
510	Program, administered by UCAR's Cooperative Programs for the Advancement of Earth System
511	Science (CPAESS) under award #NA21OAR4310383. This work was further supported an NSI
512	OCE grant 2222365 to B.H. and J.F. and NSF OCE 2049143 to J.F. Special thanks to the crew
513	and science party of the May 2022 NCC Bell M. Shimada Cruise and the Oregon State
514	University Keck Plasma Laboratory and Stable Isotope Laboratory. We also thank NOAA-
515	Fisheries for the ship time that supported data collection for this research.
516	
517	Open Research
518	All data referenced herein is available from the Dryad Data Repository at Hupp and
519	Fehrenbacher (2023).
520	
521	References
522	Alldredge, A. & Cohen, Y. (1987) Can microscale chemical patches persist in the sea?
523	Microelectrode study of marine snow, fecal pellets. Science 235, 689-691.
524	https://doi.org/10.1126/science.235.4789.689
525	Allen, K. A., Hönisch, B., Eggins, S. M., Haynes, L. L., Rosenthal, Y., & Yu, J. (2016). Trace
526	element proxies for surface ocean conditions: A synthesis of culture calibrations with
527	planktic foraminifera. Geochimica et Cosmochimica Acta, 193, 197-221.
528	https://doi.org/10.1016/j.gca.2016.08.015
529	Anand, P., Elderfield, H., & Conte, M. H. (2003). Calibration of Mg/Ca thermometry in
530	planktonic foraminifera from a sediment trap time series: Calibration of Mg/Ca

- thermometry in planktonic foraminifera. *Paleoceanography*, 18(2), n/a-n/a.
- https://doi.org/10.1029/2002PA000846
- Bauch, D., Erlenkeuser, H., Winckler, G., Pavlova, G., & Thiede, J. (2002). Carbon isotopes and
- habitat of polar planktic foraminifera in the Okhotsk Sea: the 'carbonate ion effect' under
- natural conditions. *Marine Micropaleontology*, 17.
- Bé, A.W. H., & Lott, L. (1964). Shell Growth and Structure of Planktonic Foraminifera. Science,
- 637 145(3634), 823–824. https://doi.org/10.1126/science.145.3634.823
- 638 Bé, A.W.H. (1980). Gametogenic calcification in a spinose planktonic foraminifer,
- 639 Globigerinoides sacculifer (Brady). Marine Micropaleontology, 5, 283–310.
- https://doi.org/10.1016/0377-8398(80)90014-6
- Bertlich, J., Nürnberg, D., Hathorne, E. C., de Nooijer, L. J., Mezger, E. M., Kienast, M., et al.
- 642 (2018). Salinity control on Na incorporation into calcite tests of the planktonic foraminifera
- 643 Trilobatus sacculifer evidence from culture experiments and surface sediments.
- Biogeosciences, 15(20), 5991–6018. https://doi.org/10.5194/bg-15-5991-2018
- Blanc, P.-L., & Bé, A. W. H. (1981). Oxygen-18 Enrichment of Planktonic Foraminifera Due to
- Gametogenic Calcification Below the Euphotic Zone. *Science*, 213(4513), 1247–1250.
- 647 https://doi.org/10.1126/science.213.4513.1247
- Bolton, A., & Marr, J. P. (2013). Trace element variability in crust-bearing and non-crust-bearing
- Neogloboquadrina incompta, P–D intergrade and Globoconella inflata from the Southwest
- Pacific Ocean: Potential paleoceanographic implications. *Marine Micropaleontology*, 100,
- 651 21–33. https://doi.org/10.1016/j.marmicro.2013.03.008
- Bonnin, E. A., Zhu, Z., Fehrenbacher, J. S., Russell, A. D., Hönisch, B., Spero, H. J., & Gagnon,
- A. C. (2019). Submicron sodium banding in cultured planktic foraminifera shells.
- 654 Geochimica et Cosmochimica Acta, 253, 127–141.
- https://doi.org/10.1016/j.gca.2019.03.024
- Branson, O., Read, E., Redfern, S. A. T., Rau, C., & Elderfield, H. (2015). Revisiting diagenesis
- on the Ontong Java Plateau: Evidence for authigenic crust precipitation in *Globorotalia*
- 658 tumida. Paleoceanography, 30(11), 1490–1502. https://doi.org/10.1002/2014PA002759
- Branson, O., Fehrenbacher, J.S., Vetter, L., Sadekov, A.Y., Eggins, S.M., & Spero, H.J. (2019)
- LAtools: A data analysis package for the reproducible reduction of LA-ICPMS data.
- 661 Chemical Geology, 504, 83-95. https://doi.org/10.1016/j.chemgeo.2018.10.029

- Brown, S. J., & Elderfield, H. (1996). Variations in Mg/Ca and Sr/Ca ratios of planktonic
- foraminifera caused by post depositional dissolution: Evidence of shallow Mg-dependent
- dissolution. *Paleoceanography*, 11(5), 543–551. https://doi.org/10.1029/96PA01491
- Bryan, S. P., & Marchitto, T. M. (2010). Testing the utility of paleonutrient proxies Cd/Ca and
- Zn/Ca in benthic foraminifera from thermocline waters: Cd/Ca AND Zn/Ca IN BENTHIC
- FORAMINIFERA. Geochemistry, Geophysics, Geosystems, 11(1), n/a-n/a.
- https://doi.org/10.1029/2009GC002780
- 669 Caron, D. A., Roger Anderson, O., Lindsey, J. L., Faber, W. W., & Lin Lim, E. E. (1990).
- Effects of gametogenesis on test structure and dissolution of some spinose planktonic
- foraminifera and implications for test preservation. *Marine Micropaleontology*, 16(1–2),
- 93–116. https://doi.org/10.1016/0377-8398(90)90031-G
- 673 Coplen, T.B., Kendall, C., Hopple, J., (1983). Comparison of stable isotope reference samples.
- 674 *Nature 302*, 236–238.
- Davis, C. V., Fehrenbacher, J. S., Hill, T. M., Russell, A. D., & Spero, H. J. (2017).
- Relationships Between Temperature, pH, and Crusting on Mg/Ca Ratios in Laboratory-
- 677 Grown Neogloboquadrina Foraminifera: Mg/Ca in Neogloboquadrina Foraminifera.
- 678 Paleoceanography, 32(11), 1137–1152. https://doi.org/10.1002/2017PA003111
- Davis, C.V., Fehrenbacher, J.S., Benitez-Nelson, C., & Thunell, R.C. (2020). Trace element
- heterogeneity across individual planktic foraminifera from the modern Cariaco Basin.
- *Journal of Foraminiferal Research* 50(2), 204-218.
- De Nooijer, L.J., Toyofuku, T., Oguri, K., Nomaki, H., Kitazato, H. (2008) Intracellular pH
- distribution in Foraminifera determined by the fluorescent probe HPTS. *Limnology*
- 684 *Oceanography—Methods* 6, 610–618.
- De Nooijer, L. J., Toyofuku, T. and Kitazato, H. (2009). Foraminifera promote calcification by
- 686 elevating their intracellular pH, *Proc. Natl. Acad. Sci. U. S. A.*, 106(36), 15,374–15,378,
- 687 https://doi:10.1073/pnas.0904306106
- Dekens, P. S., Lea, D. W., Pak, D. K., & Spero, H. J. (2002). Core top calibration of Mg/Ca in
- tropical foraminifera: Refining paleotemperature estimation: Core top calibration.
- 690 Geochemistry, Geophysics, Geosystems, 3(4), 1–29. https://doi.org/10.1029/2001GC000200
- Duckworth, D. L. (1977). Magnesium concentration in the tests of the planktonic foraminifer
- 692 Globorotalia truncatulinoides. Journal of Foraminiferal Research, 7(4), 304-312

- Duplessy, J. C., Bé, A. W. H., & Blanc, P. L. (1981). Oxygen and carbon isotopic composition
- and biogeographic distribution of planktonic foraminifera in the Indian Ocean.
- 695 Palaeogeography, Palaeoclimatology, Palaeoecology, 33(1–3), 9–46.
- 696 https://doi.org/10.1016/0031-0182(81)90031-6
- 697 Eggins, S., De Deckker, P., & Marshall, J. (2003). Mg/Ca variation in planktonic foraminifera
- tests: implications for reconstructing palaeo-seawater temperature and habitat migration.
- Earth and Planetary Science Letters, 212(3-4), 291-306. https://doi.org/10.1016/S0012-
- 700 821X(03)00283-8
- 701 Elderfield, H. & Ganssen, G. (2000). Past temperature and $\delta^{18}O$ of surface ocean waters inferred
- from foraminiferal Mg/Ca ratios. *Nature*, 405, 442-445.
- Fehrenbacher, J. S., Russell, A. D., Davis, C. V., Gagnon, A. C., Spero, H. J., Cliff, J. B., et al.
- 704 (2017). Link between light-triggered Mg-banding and chamber formation in the planktic
- foraminifera Neogloboquadrina dutertrei. *Nature Communications*, 8(1), 15441.
- 706 https://doi.org/10.1038/ncomms15441
- Fehrenbacher, J. S., Russell, A. D., Davis, C. V., Spero, H. J., Chu, E., & Hönisch, B. (2018).
- Ba/Ca ratios in the non-spinose planktic foraminifer *Neogloboquadrina dutertrei*: Evidence
- for an organic aggregate microhabitat. *Geochimica et Cosmochimica Acta*, 236, 361–372.
- 710 https://doi.org/10.1016/j.gca.2018.03.008
- 711 Fritz-Endres, T., Fehrenbacher, J. S., Russell, A. D., & Cynar, H. (2022). Increased Productivity
- in the Equatorial Pacific During the Deglaciation Inferred from the Ba/Ca Ratios of Non-
- 713 Spinose Planktic Foraminifera. *Paleoceanography and Paleoclimatology*, 37(12).
- 714 https://doi.org/10.1029/2022PA004506
- Greco, M., Jonkers, L., Kretschmer, K., Bijma, J., & Kucera, M. (2019). Depth habitat of the
- 716 planktonic foraminifera *Neogloboquadrina pachyderma* in the northern high latitudes
- explained by sea-ice and chlorophyll concentrations. *Biogeosciences*, 16(17), 3425–3437.
- 718 https://doi.org/10.5194/bg-16-3425-2019
- Hamilton, C.P., Spero, H.J., Bijma, J., & Lea, D.W. (2008) Geochemical investigation of
- gametogenic calcite addition in the planktonic foraminifera *Orbulina universa*. *Marine*
- 721 *Micropaleontology* 68(3), 256-267. https://doi.org/10.1016/j.marmicro.2008.04.003
- Hathorne, E. C., James, R. H., & Lampitt, R. S. (2009). Environmental versus biomineralization
- controls on the intratest variation in the trace element composition of the planktonic

- foraminifera *G. inflata* and *G. scitula*: Environmental versus biomineral controls.
- 725 *Paleoceanography*, 24(4). https://doi.org/10.1029/2009PA001742
- Hebel D., Knauer G. A. & Martin J. H. (1986) Trace-metals in large agglomerates (marine
- snow). Journal of Plankton. Research 8, 819–824.
- Hemleben, C., Spindler, M., Anderson, O.R., 1989. Modern Planktonic Foraminifera. Springer,
- 729 New York, 363 pp.
- Hönisch, B., Allen, K. A., Lea, D. W., Spero, H. J., Eggins, S. M., Arbuszewski, J., et al. (2013).
- 731 The influence of salinity on Mg/Ca in planktic foraminifers Evidence from cultures, core-
- top sediments and complementary δ18O. Geochimica et Cosmochimica Acta, 121, 196–213.
- 733 https://doi.org/10.1016/j.gca.2013.07.028
- Hupp, B., & Fehrenbacher, J. (2023). LA-ICP-MS Neogloboquadrina pachyderma spectral files
- from "Geochemical differences between alive, uncrusted and dead, crusted shells of
- Neogloboquadrina pachyderma: Implications for paleoreconstruction" [Dataset]. Dryad.
- 737 https://doi.org/10.5061/dryad.gtht76hsk
- Hupp, B., & Fehrenbacher, J. (2023). Stable isotope geochemistry of recently deceased and alive
- Neogloboquadrina pachyderma shells collected from offshore Oregon Coast (USA)
- 740 [Dataset]. PANGAEA. < future link>
- Jochum, K. P., Weis, U., Stoll, B., Kuzmin, D., Yang, Q., Raczek, I., et al. (2011). Determination
- of Reference Values for NIST SRM 610-617 Glasses Following ISO Guidelines.
- Geostandards and Geoanalytical Research, 35(4), 397–429. https://doi.org/10.1111/j.1751-
- 744 908X.2011.00120.x
- Johnstone, H. J. H., Schulz, M., Barker, S., & Elderfield, H. (2010). Inside story: An X-ray
- computed tomography method for assessing dissolution in the tests of planktonic
- 747 foraminifera. *Marine Micropaleontology*, 77(1–2), 58–70.
- 748 https://doi.org/10.1016/j.marmicro.2010.07.004
- Jonkers, L., de Nooijer, L. J., Reichart, G.-J., Zahn, R., & Brummer, G.-J. A. (2012).
- 750 Encrustation and trace element composition of *Neogloboquadrina dutertrei* assessed from
- single chamber analyses implications for paleotemperature estimates. *Biogeosciences*,
- 752 9(11), 4851–4860. https://doi.org/10.5194/bg-9-4851-2012

- Jonkers, L., Buse, B., Brummer, G-J., A. Hall, I.R. (2016) Chamber formation leads to Mg/Ca
- banding in the planktonic foraminifer *Neogloboquadrina pachyderma*. Earth and Planetary
- 755 Science Letters 451, 177-184.
- Jørgensen, B.B., Erez, J., Revsbech, P. & Cohen, Y. (1985) Symbiotic photosynthesis in a
- 757 planktonic foraminiferan, Globigerinoides sacculifer (Brady), studied with microelectrodes
- 758 1. *Limnology and Oceanography* 30(6), 1253-1267.
- Katz, M. E., Cramer, B. S., Franzese, A., Hönisch, B., Miller, K. G., Rosenthal, Y., & Wright, J.
- D. (2010). Traditional and emerging geochemical proxies in foraminifera. *The Journal of*
- 761 Foraminiferal Research, 40(2), 165–192. https://doi.org/10.2113/gsjfr.40.2.165
- Kim, S.-T., & O'Neil, J. R. (1997). Equilibrium and nonequilibrium oxygen isotope effects in
- synthetic carbonates. *Geochimica et Cosmochimica Acta*, 61(16), 3461–3475.
- 764 https://doi.org/10.1016/S0016-7037(97)00169-5
- Köhler-Rink, S. & Kühl, M. (2000) Microsensor studies of photosynthesis and respiration in
- larger symbiotic foraminifera. I The physico-chemical microenvironment of *Marginopora*
- vertebralis, Amphistegina lobifera and Amphisorus hemprichii. Marine Biology 137, 473-
- 768 486.
- Kozdon, R., Ushikubo, T., Kita, N. T., Spicuzza, M., & Valley, J. W. (2009). Intratest oxygen
- isotope variability in the planktonic foraminifer *N. pachyderma*: Real vs. apparent vital
- effects by ion microprobe. *Chemical Geology*, 258(3–4), 327–337.
- 772 https://doi.org/10.1016/j.chemgeo.2008.10.032
- Lane, M. K., Fehrenbacher, J. S., Fisher, J. L., Fewings, M. R., Crump, B. C., Risien, C. M., et
- al. (2023). Planktonic foraminiferal assemblages reflect warming during two recent mid-
- 1775 latitude marine heatwayes. Frontiers in Marine Science, 10, 1155761.
- 776 https://doi.org/10.3389/fmars.2023.1155761
- Lea, D. W., Mashiotta, T. A., & Spero, H. J. (1999). Controls on magnesium and strontium
- uptake in planktonic foraminifera determined by live culturing. Geochimica et
- 779 Cosmochimica Acta, 63(16), 2369–2379. https://doi.org/10.1016/S0016-7037(99)00197-0
- 780 Livsey, C.M., Kozdon, R., Bauch, D., Brummer, G-J.A., Jonkers, L., Orland, I., Hill, T.M., &
- Spero, H.J. (2020) High-resolution Mg/Ca and δ^{18} O patterns in modern Neogloboquadrina
- pachyderma from the Fram Strait and Irminger Sea. *Paleoceanography and*
- 783 Paleoclimatology 35, e2020PA003969. https://doi.org/10.1029/2020PA003969

- Longerich, H. P., Jackson, S. E., & Günther, D. (1996). Inter-laboratory note. Laser ablation
- inductively coupled plasma mass spectrometric transient signal data acquisition and analyte
- concentration calculation. *Journal of analytical atomic spectrometry* 11(9), 899-904.
- Marchitto, T. M., Curry, W. B., & Oppo, D. W. (2000). Zinc concentrations in benthic
- foraminifera reflect seawater chemistry. *Paleoceanography*, 15(3), 299–306.
- 789 https://doi.org/10.1029/1999PA000420
- Martin, P. A., & Lea, D. W. (2002). A simple evaluation of cleaning procedures on fossil benthic
- foraminiferal Mg/Ca. Geochemistry, Geophysics, Geosystems, 3(10), 8 p. https://doi.org/
- 792 10.1029/2001GC000280
- 793 Martínez-Botí, M. A., Mortyn, P. G., Schmidt, D. N., Vance, D., & Field, D. B. (2011). Mg/Ca
- in foraminifera from plankton tows: Evaluation of proxy controls and comparison with core
- 795 tops. Earth and Planetary Science Letters, 307(1–2), 113–125.
- 796 https://doi.org/10.1016/j.epsl.2011.04.019
- Meilland, J., Siccha, M., Kaffenberger, M., Bijma, J., & Kucera, M. (2021). Population dynamics
- and reproduction strategies of planktonic foraminifera in the open ocean. *Biogeosciences*,
- 799 *18*(20), 5789–5809. https://doi.org/10.5194/bg-18-5789-2021
- Mezger, E.M., de Nooijer, L.J., Boer, W., Brummer, G.-J., A., & Reichart G.-J. (2016) Salinity
- controls on Na incorporation in Red Sea planktonic foraminifera. *Paleoceanography 31*,
- 802 1562-1582.
- Mulitza, S., Dürkoop, A., Hale, W., Wefer, G., & Stefan Niebler, H. (1997). Planktonic
- foraminifera as recorders of past surface-water stratification. *Geology*, 25(4), 335.
- 805 https://doi.org/10.1130/0091-7613(1997)025<0335:PFAROP>2.3.CO;2
- Niebler, H. S., Hubberten, H. W., & Gersonde, R. (1999). Oxygen isotope values of planktic
- foraminifera: a tool for the reconstruction of surface water stratification. *Use of Proxies in*
- *Paleoceanography: examples from the South Atlantic*, 165-189.
- Nürnberg, D., Bijma, J., & Hemleben, C. (1996) Assessing the reliability of magnesium in
- foraminiferal calcite as a proxy for water mass temperatures. Geochemica et Cosmochimica
- 811 *Acta*, 60(5), 803-814.
- Ortiz, J.D., Mix, A. C., Rugh, W., Watkins, J. M., & Collier, R. W. (1996). Deep-dwelling
- planktonic foraminifera of the northeastern Pacific Ocean reveal environmental control of

814 oxygen and carbon isotopic disequilibria. Geochimica et Cosmochimica Acta, 60(22), 815 4509–4523. https://doi.org/10.1016/S0016-7037(96)00256-6 816 Ortiz, Joseph D., & Mix, A. C. (1992). The spatial distribution and seasonal succession of 817 planktonic foraminifera in the California Current off Oregon, September 1987 – September 818 1988. Geological Society, London, Special Publications, 64(1), 197–213. 819 https://doi.org/10.1144/GSL.SP.1992.064.01.13 820 Pena, L.D., Cacho, I., Calvo, E., Pelejero, C., Eggins, S., & Sadekov, A. (2008). Characterization 821 of contaminant phases in foraminifera carbonates by electron microprobe mapping. 822 Geochemistry, Geophysics, Geosystems, 9(7), 12 p. https://doi:10.1029/2008GC002018 823 Richey, J. N., Fehrenbacher, J. S., Reynolds, C. E., Davis, C. V., & Spero, H. J. (2022). Barium 824 enrichment in the non-spinose planktic foraminifer, Globorotalia truncatulinoides. 825 Geochimica et Cosmochimica Acta, 333, 184–199. 826 https://doi.org/10.1016/j.gca.2022.07.006 827 Rink, S., Kühl, M., Bijma, J. & Spero, H.J., 1998. Microsensor studies of photosynthesis and 828 respiration in the symbiotic foraminifer Orbulina universa. Marine Biology 131, 583-595. 829 Rosenthal, Y., Lohmann, G. P., Lohmann, K. C., & Sherrell, R. M. (2000). Incorporation and 830 preservation of Mg in Globigerinoides sacculifer: implications for reconstructing the temperature and ¹⁸ O/ ¹⁶ O of seawater. *Paleoceanography*, 15(1), 135–145. 831 832 https://doi.org/10.1029/1999PA000415 833 Russell, A. D., Hönisch, B., Spero, H. J., & Lea, D. W. (2004). Effects of seawater carbonate ion 834 concentration and temperature on shell U, Mg, and Sr in cultured planktonic foraminifera. 835 Geochimica et Cosmochimica Acta, 68(21), 4347–4361. 836 https://doi.org/10.1016/j.gca.2004.03.013 837 Sadekov, A. Yu., Eggins, S. M., & De Deckker, P. (2005). Characterization of Mg/Ca 838 distributions in planktonic foraminifera species by electron microprobe mapping: Mg/Ca in 839 Planktonic Foraminifera. Geochemistry, Geophysics, Geosystems, 6(12), n/a-n/a. 840 https://doi.org/10.1029/2005GC000973 841 Sadekov, A. Yu., Eggins, S. M., Klinkhammer, G. P., & Rosenthal, Y. (2010). Effects of seafloor 842 and laboratory dissolution on the Mg/Ca composition of Globigerinoides sacculifer and 843 Orbulina universa tests — A laser ablation ICPMS microanalysis perspective. Earth and 844 Planetary Science Letters, 292(3–4), 312–324. https://doi.org/10.1016/j.epsl.2010.01.039

845	Schiebel, R., & Hemleben, C. (2017). Planktic Foraminifers in the Modern Ocean. Berlin,
846	Heidelberg: Springer Berlin Heidelberg. https://doi.org/10.1007/978-3-662-50297-6
847	Schweitzer, P. N., & Lohmann, G. P. (1991). Ontogeny and habitat of modern menardiiform
848	planktonic foraminifera. The Journal of Foraminiferal Research, 21(4), 332-346.
849	https://doi.org/10.2113/gsjfr.21.4.332
850	Spero, H.J., Bijma, J., Lea, D.W., & Bemis, B.E. (1997). Effect of seawater carbonate
851	concentration on foraminiferal carbon and oxygen isotopes. Nature 390, 497-500.
852	Spero, H.J., Eggins, S.M., Russell, A.D., Vetter, L., Kilburn, M.R., Hönisch, B. (2015). Timing
853	and mechanism for intratest Mg/Ca variability in a living planktic foraminifer. Earth and
854	Planetary Science Letters 409, 32-42, https://doi.org/10.1016/j.epsl.2014.10.030.
855	Stangeew, E. (2001). Distribution and Isotopic Composition of Living Planktonic Foraminifera
856	N. pachyderma (sinistral) and T. quinqueloba in the High Latitude North Atlantic, 98.
857	Steinhardt, J., Cléroux, C., Ullgren, J., de Nooijer, L., Durgadoo, J.V., Brummer, GJ., Reichart,
858	GJ. (2014). Anti-cyclonic eddy imprint on calcite geochemistry of several planktonic
859	foraminiferal species in the Mozambique Channel. Marine Micropaleontology 113, 20-33.
860	Steinhardt, J., de Nooijer, L. L. J., Brummer, GJ., & Reichart, GJ. (2015). Profiling planktonic
861	foraminiferal crust formation: Profiling Planktic Foraminiferal Crust. Geochemistry,
862	Geophysics, Geosystems, 16(7), 2409–2430. https://doi.org/10.1002/2015GC005752
863	Takagi, H., Kimoto, K., Fujiki, T., Saito, H., Schmidt, C., Kucera, M., & Moriya, K. (2019).
864	Characterizing photosymbiosis in modern planktonic foraminifera. Biogeosciences, 16(17),
865	3377–3396. https://doi.org/10.5194/bg-16-3377-2019
866	Vergnaud Grazzini, C. (1976). Non-equilibrium isotopic compositions of shells of planktonic
867	foraminifera in the Mediterranean Sea. Palaeogeography, Palaeoclimatology,
868	Palaeoecology, 20(4), 263–276. https://doi.org/10.1016/0031-0182(76)90007-9
869	Wycech, J., Kelly, D. C., & Marcott, S. (2016). Effects of seafloor diagenesis on planktic
870	foraminiferal radiocarbon ages. Geology, 44(7), 551–554. https://doi.org/10.1130/G37864.1
871	
872	Figure Captions
873	Figure 1. Representative examples of a) a mixture of live, uncrusted (LU) and dead, crusted
874	(DC) shells in a plankton tow sample, b) a live-caught uncrusted Neogloboquadrina pachyderma
875	shell that has been cleaned to remove the colorful cytoplasm, and c) a cleaned, dead, crusted

876 shell of N. pachyderma. Scale bars are equal to 100 μm. d) A schematic illustrating the relative 877 position of the outer whorl chambers examined in this study. 878 879 Figure 2. Bathymetric map showing the location of the two collection sites (NH85, NH45) off 880 the Oregon coast. Distance scale bar is in kilometers (km). 881 882 Figure 3. Profiles of the uppermost 500 m of the water column from NH85 (solid line) and 883 NH45 (dashed line) showing the a) temperature, b) salinity, c) chlorophyll content, and d) 884 dissolved oxygen measured from CTD casts on the day of plankton tow collections. 885 886 **Figure 4.** Boxplots showing the distributions of *N. pachyderma* TE/Ca data from each individual 887 chamber in the final whorl (F0, F1, F2, F3) and the whole-shell average for the alive-caught, 888 uncrusted shells (pink) and dead, crusted shells (blue). a) Mg/Ca, b) Ba/Ca, c) Na/Ca, d) Mn/Ca, 889 e) Sr/Ca, and f) Zn/Ca. Red stars denote significant differences between the crusted and 890 uncrusted populations (Mann-Whitney test, p-value <0.05). 891 892 Figure 5. Example TE/Ca depth profile for a-b) a crusted specimen (Shell #100, F2 chamber) 893 and c-d) an uncrusted specimen (Shell #4, F2 chamber). 894 895 **Figure 6.** Boxplots showing the $\Delta TE/Ca_{inner-outer}$ distributions, where $\Delta TE/Ca_{inner-outer}$ values are 896 calculated as the difference between the average inner 50% of a TE/Ca spectrum minus the 897 average of the outer 50% of the same TE/Ca spectrum for each chamber of a given shell. a) 898 Mg/Ca, b) Ba/Ca, c) Na/Ca, d) Mn/Ca, e) Sr/Ca, and f) Zn/Ca. Distributions derived from 899 uncrusted shells are shown in pink whereas distributions of crusted shells are shown in blue. 900 901 Figure 7. Boxplots of whole-shell average a) Mg/Ca, b) Na/Ca, c) Sr/Ca, d) Ba/Ca, e) Mn/Ca 902 and f) Zn/Ca values of uncrusted shells (yellow) to the inner 50% average (blue) and outer 50% 903 average (purple) of the crusted shells. Significant differences were denoted with a red star 904 (Mann-Whitney test, p-value < 0.05).

Figure 8. Boxplots of stable a) carbon (δ^{13} C) and b) oxygen (δ^{18} O) isotope values for the uncrusted (pink) and crusted (blue) shells. The uncrusted and crusted populations were found to be significantly different (Student's t-test) in both their carbon and oxygen isotopic compositions, as denoted by the red stars. c) A cross plot of the carbon and oxygen isotope values for uncrusted shells (pink circles) and crusted shells (blue circles), and the $\delta^{13}C_{DIC}$ and δ^{18} O_{calcite} measured or calculated, respectively, from the water samples collected from NH45 (black diamonds) and NH85 (white diamonds). The numbers labeling each diamond denote the depth (m) at which the water sample was collected. The $\delta^{18}O_{calcite}$ values in panel C are the predicted δ^{18} O of calcite precipitated under equilibrium at each water depth as determined from measured $\delta^{18}O_{sw}$ and temperature, using the Kim and O'Neil (1997) equation. Note that each shell data point represents an analysis of two to three shells of the same life stage (dead vs. live) from the same plankton tow that were pooled together. Figure 9. Comparison of a) carbon and b) oxygen isotope data of crusted (blue boxplots) and uncrusted (pink boxplots) shells to the $\delta^{13}C_{DIC}$ and $\delta^{18}O_{calcite}$ profiles. The $\delta^{18}O$ equilibrium calcite profile was calculated using the equation from Kim and O'Neil (1997). Red dots and associated labels demarcate the depth of crusting assuming various mixing scenarios of crust and ontogenetic calcite (Section 4.2). Mixing scenarios and estimated depths of crusting using the δ^{13} C data is included as an inlayed table in panel A.

Tables and Table Captions

935

944 945

946947

948

936 Table 1. Summary of TE/Ca differences observed between the crust and ontogenetic calcites as 937 found in the published literature. TE/Ca comparisons are labeled as the crust calcite either being found to be lower, higher, or no difference (ND) in TE/Ca values when compared to the 938 ontogenetic calcite of the same shell. References are as follows: ¹Eggins et al., 2003; ²this study; 939 ³Davis et al., 2017; ⁴Sadekov et al., 2005; ⁵Bolton & Marr, 2013; ⁶Pena et al., 2008; ⁷Jonkers et 940 al., 2012; 8Steinhardt et al., 2015; 9Duckworth, 1977; 10Hathorne et al., 2009; 11Brown and 941 Elderfield, 1996; ¹²Branson et al., 2015; ¹³Elderfield and Ganssen, 2000; ¹⁴Nürnberg et al., 942 1996¹⁴; ¹⁵Rosenthal et al., 2000; ¹⁶Bertlich et al, 2018. 943

Species	Mg/Ca	Na/Ca	Sr/Ca	Ba/Ca	Mn/Ca	Zn/Ca
Neogloboquadrina	Lower ^{1,3} ,	Lower ²	Lower ²	Lower ²	Lower ²	Lower ²
pachyderma	ND^2					
N. incompta	Lower ^{3,4,}	-	ND^2	_	_	_
N. pachyderma- dutertrei	Lower ⁵	_	ND^5	_	_	-
(P-D) intergrade						
N. dutertrei	Lower ^{1,4,} 6,7,8		ND ^{1,6}	Lower ¹	Lower ^{1,6,}	Lower ¹
Globorotalia	Lower ^{4,9}					
truncatulinoides						
G. inflata	Lower ^{5,10}	_	$ND^{5,10}$	Lower ¹⁰	Lower ¹⁰	-
G. scitula	Lower ^{8,10}		ND^{10}	Lower ¹⁰	Lower ¹⁰	
G. tumida	Lower ^{11,1}		ND ¹²			
G. menardii	Lower ⁴					
Globogerina bulloides	Lower ¹³					
Trilobatus sacculifer	Higher ¹⁴ ;	Higher ¹⁶	ND^1	Lower ¹	Lower ¹	Lower ¹
	Lower ^{1,15}					
	, ND ^{1,11}					
Globigerinoides ruber	ND ^{1,4}		ND^1	ND^1	ND ¹	ND^1
G. conglobatus	Lower ⁴					
Pulleniatina	Lower ⁸					
obliguiloculata*						
Orbulina universa	Lower ⁴					

^{*} This comparison was not between the gametogenic crust and early ontogenetic calcite, but rather between the cortex and early ontogenetic calcite.

Table 2. Carbon ($\delta^{13}C_{DIC}$) and oxygen ($\delta^{18}O_{sw}$) isotope values measured from the seawater samples collected from each site. Temperatures measured from the CTD and predicted $\delta^{18}O$ values for equilibrium calcite ($\delta^{18}O_{calcite}$) using the equation from Kim and O'Neil (1997) are also shown.

Site	Latitude (°N)	Longitude (°W)	Depth Sampled (m)	δ ¹³ Cdic (‰VPDB)	δ ¹⁸ O _{sw} (%VSMOW)	Temperature (°C)	Calculated Equilibrium Calcite δ ¹⁸ O _{calcite} (‰VPDB)
NH45	44.6517	-125.117	5	1.34	-0.98	10.88	-0.36
			25	1.34	-0.92	10.83	-0.29
			50	0.39	-0.64	9.04	0.39
			100	-0.27	-0.26	8.58	0.88
			150	-0.46	-0.16	7.86	1.14
			250	-0.49	-0.19	6.70	1.38
			500	-0.57	-0.18	5.01	1.78
NH85	44.6517	-126.05	5	1.28	-0.84	10.93	-0.23
			25	1.26	-0.87	10.85	-0.24
			50	0.57	-0.66	10.02	0.15
			100	-0.29	-0.25	8.75	0.85
			150	-0.45	-0.15	8.01	1.11
			250	-0.45	-0.11	7.03	1.38
			500	-0.47	-0.14	5.23	1.77

Figure 1

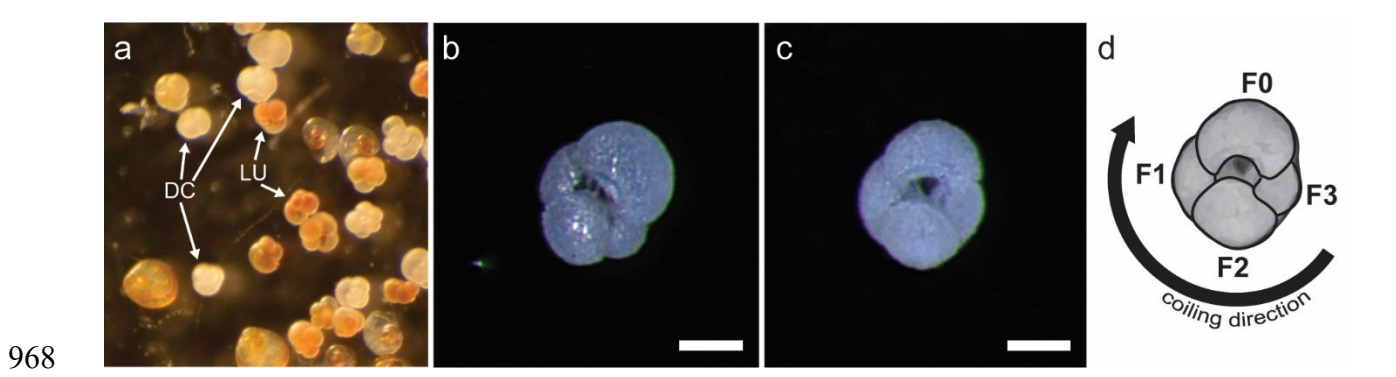


Figure 2.

